Current Applied Physics 20 (2020) 1429–1434

Contents lists available at ScienceDirect

Current Applied Physics

journal homepage: www.elsevier.com/locate/cap

# Phase composition and magnetic structure in nanocrystalline ferromagnetic Fe–N–O films

E.N. Sheftel, V.A. Tedzhetov, E.V. Harin *, G.Sh Usmanova

*Baikov Institute of Metallurgy and Materials Science, Russian Academy of Sciences, Leninsky Prospect 49, Moscow, 119334, Russia*

ARTICLE INFO

*Keywords:*
Magnetic measurements
Phase diagrams
Magnetic films and multilayers
X-ray diffraction
Nanostructured materials
Vapor deposition

ABSTRACT

The chemical and phase compositions and structure of the Fe–N–O films produced by reactive dc magnetron sputtering (in Ar or Ar + $N_2$ gas mixture atmospheres) under different conditions (energy parameters of magnetron, residual pressure in the magnetron chamber after preliminary pumping, operating pressure in gas mixture) have been investigated by energy-dispersive X-ray spectroscopy, X-ray diffraction analysis, and vibrating sample magnetometry. Impurity of nitrogen and oxygen, which are present in the sputtered films, participate in the formation of their phase composition and determine its features. Some phenomena inherent in the nanocrystalline films in the metastable state were found. These are the formation of supersaturated bcc interstitial αFe-based solid solution and precipitation of α' nitrous martensite with bct crystal lattice. The magnetic structure of the Fe–N–O films, which is characterized by the existence of stochastic domains discovered by correlation magnetometry method, is discussed in terms of the random anisotropy model. It was found that two modes of the magnetic anisotropy field of stochastic domains are formed, which determine the existence of two modes of the coercive field found in the magnetic hysteresis loops.

## 1. Introduction

High-induction Fe-based ferromagnets with the nanocomposite structure are promising materials for miniature high-performance devices for weak magnetic fields in a wide range of applications [1]. In particular, in the Fe–N system there are αFe and $Fe_{16}N_2$ phases [2] with the highest saturation induction at room temperature [3]. Given the trend towards device miniaturization, films and foils exhibit the unique combination of properties, such as the high saturation induction, high hardness, and thermal stability of properties [4].

The preparation of the films by reactive magnetron sputtering of a Fe target in an Ar + $N_2$ gas mixture can lead to uncontrolled contamination of films with oxygen and nitrogen. As a result, the chemical composition of films and the concentration range of the existence of phases can vary.

The magnetic hysteresis properties of such alloys can be most fully explained using the random anisotropy model (RAM) [5]. This model assumes that the easy magnetization axes of individual grains of radius $R_c$ (or local magnetically homogeneous regions of radius $R_c$ in the amorphous phase) are randomly oriented and the distribution of local magnetization can be described by some autocorrelation function. An important parameter of this function is the magnetic autocorrelation radius $R_L$, which is the size of the region in which the magnetization is relatively uniform. In nano- and amorphous alloys, an extreme decrease in the coercive field relative to the local magnetic anisotropy field is realized under the condition $R_L \gg R_c$. This condition exists in RAM in the case when the length of the ferromagnetic exchange interaction exceeds the size $R_c$, which causes averaging of the local magnetic anisotropy in the volume of radius $R_{L1}$ (stochastic magnetic domain). Note that under certain conditions, the material may additionally implement other reasons for the existence of a second magnetic autocorrelation radius of size $R_{L2}$ (second stochastic magnetic domain).

In this regards, investigations of the chemical and phase compositions, structure, and magnetic structure of Fe–N–O films produced by magnetron sputtering under different conditions (energy parameters of magnetron, residual pressure in the magnetron chamber after preliminary pumping, operating pressure in gas mixture) are of importance from the viewpoint of academic interest and practical recommendations and are the subject of the presented work.

## 2. Experimental

The Fe–N–O films on glass substrates (1.5 mm thick) were prepared

* Corresponding author.
*E-mail address:* ekharin@imet.ac.ru (E.V. Harin).

https://doi.org/10.1016/j.cap.2020.09.009
Received 28 February 2020; Received in revised form 3 September 2020; Accepted 23 September 2020
Available online 6 October 2020

by dc reactive magnetron sputtering using an installation equipped with an oil diffusion pump. The introduction of nitrogen to the films was realized by sputtering of a Fe target in an Ar + $N_2$ gas mixture with a variable $N_2/(Ar + N_2)$ volume ratio. Sputtering conditions were: voltage 390 V, current 1.5 A, deposition time 10 min. Table 1 shows other preparation conditions. The thickness of deposited films was determined using a Fischerscope X-ray fluorescence spectrometer (Table 1).

The chemical composition of the films was determined by energy-dispersive X-ray (EDX) spectroscopy using a Hitachi TM3000 scanning electron microscope equipped with an EDX Bruker Quantax 70 attachment (the accuracy of determination is ±2.5 at.%).

The phase and structural states of the films were studied by X-ray diffraction (XRD) using a Rigaku Ultima IV diffractometer equipped with a graphite monochromator, the Bragg-Brentano geometry, and Cu-Kα radiation. The radiation was recorded using scintillation and semiconductor detectors. The primary processing of XRD patterns was performed using an original software [6] and full-profile Rietveld analysis. For a qualitative phase analysis, a database of International Centre for Diffraction Data (ICDD) was used. Using the XRD patterns, the phase composition and the grain size $2R_c$ were determined.

Hysteresis loops were measured on a LakeShore 7407 vibrating sample magnetometer in fields up to 16 kOe. The parameters of the magnetic structure were determined by the method of correlation magnetometry [7].

## 3. Results and discussion

### 3.1. Chemical composition of the films under study

The films were found to be characterized by the high oxygen content (~20 at.%) and the low nitrogen content (from 4.8 to 8.3 at.%, Table 1). Under conditions of the present experiment, the films contain impurity oxygen, the content of which decreases as the residual pressure $P_0$ (in the magnetron chamber after preliminary pumping) decreases (Table 1, Fig. 1). Note that in addition to the residual pressure $P_0$, the pressure of the working mixture $P_{Ar+N2}$ (Table 1) also affects the nitrogen and oxygen content in the films.

This means that during deposition the conditions for the absorption of residual (in the magnetron chamber) gas atoms on the growing film are realized. Thus, under conditions of the present experiment actually the multicomponent films of the Fe–N–O system are prepared.

### 3.2. Phase composition and structure of the films under study

According to the XRD data, during condensation the nanocrystalline structure forms in the films, which is two-phase (αFe + $Fe_3O_4$) if the nitrogen content is relatively low (Fig. 2a). As the nitrogen content increases, the three-phase structure (αFe/Fe(N) + $Fe_3O_4$ + α′) forms: αFe ferromagnetic phase transforms into bcc Fe(N) solid solution (the bcc phase lattice parameter increases, Fig. 2b), ferromagnetic α′ nitrous martensite with body-centered tetragonal (bct) lattice appears (Fig. 2a), and $Fe_3O_4$ oxide phase with fcc lattice forms. It should be noted that the content of α' phase rises with increasing the nitrogen content, whereas the $Fe_3O_4$ oxide phase content is unchanged and is ~8–16 vol% in all films.

**Table 1**
Magnetron sputtering conditions, thickness, and chemical composition.

| $N_2/(Ar + N_2)$, vol % | $P_0$, Pa | $P_{Ar+N2}$, Pa | Thickness, μm | Chemical composition, at.% | | |
|---|---|---|---|---|---|---|
| | | | | Fe | N | O |
| 0 | 0.128 | 1.42 | 0.69 ± 0.02 | 72.4 | 4.8 | 22.8 |
| 10 | 0.085 | 1.23 | 0.55 ± 0.01 | 76.9 | 4.8 | 18.3 |
| 13 | 0.112 | 1.20 | 0.49 ± 0.03 | 76.2 | 4.9 | 18.9 |
| 17 | 0.120 | 1.20 | 0.43 ± 0.03 | 72.0 | 6.6 | 21.4 |
| 32 | 0.125 | 0.82 | 0.48 ± 0.03 | 71.8 | 8.3 | 19.9 |

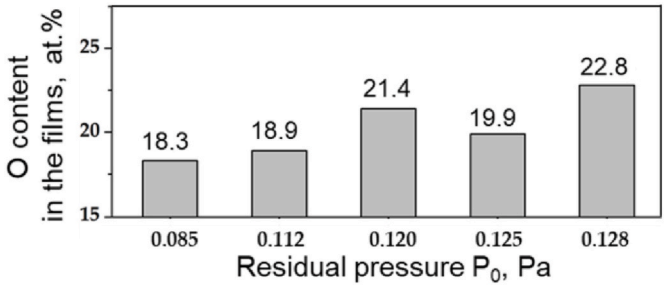


**Fig. 1.** Dependence of the oxygen content in the films under study on the residual pressure $P_0$ in the magnetron chamber after preliminary pumping.

Bct α′ nitrous martensite is rarely found in films [8], therefore we consider it in more detail. Bct α′ is an ordered solid solution of nitrogen in αFe [9], and it is sometimes referred to as the $Fe_{10}N$ phase [10–12]. Bct α′ is formed at temperatures of 380–635 °C [11] and remains stable above 600 °C [12]. According to the data from the ICDD database, the phase has the space group I4/mmm, the most intense diffraction peak is (101) at an angle of 2θ 43.2° (Cu-Kα radiation). However, in the studied films the peaks (112) and (211) are the most intense, which indicates the presence of texture (Figs. 2a and 3). In the studied films the α 'phase has a lattice parameters $a$ of 2.848–2.856 Å and $c$ 3.075–3.090 Å (Table 2), which according to the data [9] correspond to the content of 7–9 at.% N in this phase. Considering that the volume fraction of α′ phase in the films does not exceed 51%, about a half of the nitrogen is in this phase (Table 1). This leads us to the idea of the need for more careful controlling of the introduction of nitrogen into films in the future. Note that according to Ref. [9], an increase in the lattice parameter $a$ and a decrease in $c$ (as we see from Table 2 with an increase in the $N_2$ percentage) means a decrease in the nitrogen concentration in this phase. Thus, with an increase in the concentration of the $N_2$ percentage, an increase in the volume fraction of α' phase and a simultaneous decrease in the nitrogen concentration in it occur.

The nitrogen solubility in αFe in the equilibrium Fe–N system is only 0.4 at.% at 592 °C [9]. The obtained lattice parameter data (Fig. 2b) indicate the increase in the nitrogen solubility in αFe up to 4 at.% (as well as our data of [13]) and formation of supersaturated solid solutions of nitrogen in αFe.

It should be noted, that the lattice parameter of the αFe phase in the films under study is found to be less than the tabulated value for αFe (2.8664 Å, Fig. 2b). Such an effect is observed also for a number of nanocrystalline films and coatings of different compositions [14,15]. There is still no reliable explanation of this phenomenon. At the same time, according to the data [14], internal compressive stresses formed in nanocrystalline TiN coatings cause a decrease in the lattice parameter of TiN.

All prepared films are nanocrystalline. The grain size of the bcc αFe-based phase in the films decreases from ~12 to ~6 nm as the nitrogen content in the film and, therefore, in the bcc solid solution increases (Fig. 2b). This is explained by the lower diffusion mobility of atoms in the αFe(N) solid solution, which determines the grain growth and grain size, as compared to that in αFe.

The grain size of the fcc $Fe_3O_4$ phase precipitated in all films remains unchanged (9.4 ± 0.3 nm). The α' phase in the films is characterized by the lowest grain size (5–7 nm), which is unchanged for all compositions.

### 3.3. Magnetic structure of the films under study

The saturation magnetization $Ms$ of the studied films is 1450 ± 150 G (Fig. 4a, gauss = emu/cm$^3$). If it is hypothetically assumed that such a saturation magnetization is associated only with a solid solution of nitrogen in αFe, then according to our earlier data [13], the films should

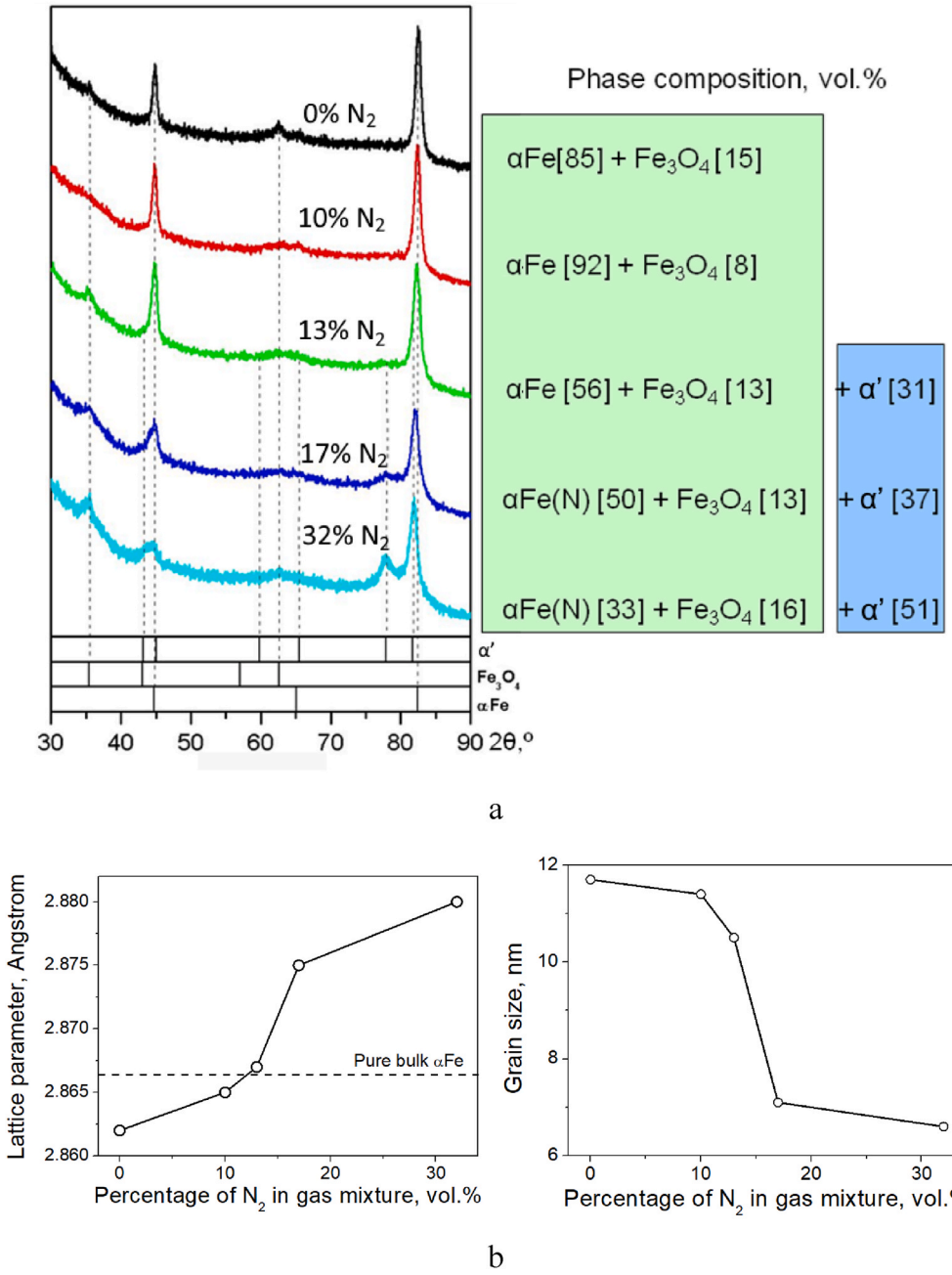


**Fig. 2.** XRD patterns of the films under study (a) and the dependences of the crystal lattice parameter and the grain size of bcc phase in the films under study on the concentration of $N_2$ in gas mixture during magnetron deposition (b). Solid lines on (b) are guides for the eyes.

contain no more than 3 at.% N. Actually (Table 1) the nitrogen content is 2–3 times higher, which means the saturation magnetization of the α' phase is greater than or equal to αFe.

To evaluate the saturation magnetization of the α′ phase, we were guided by the following considerations. We assume that the saturation magnetization of $Fe_3O_4$ is the same in all films and is equal to $M_s^{Fe3O4} = 480$ G [16]. Then the saturation magnetization of the films not containing the α ' phase (Fig. 2a) is

$$M_s = M_s^{Fe3O4} \cdot V_{Fe3O4} + M_s^{\alpha Fe(N)} \cdot (100 - V_{Fe3O4}), \quad (1)$$

where $V_{Fe3O4}$ is volume fraction of $Fe_3O_4$ phase, vol%. Taking into account that we do not know the exact nitrogen content in the αFe(N) phase, we cannot use at this step the dependence $M_s^{\alpha Fe(N)} = f(N, at.\%)$ obtained in Ref. [13]. But we can substitute the parameters of the films that do not contain the α′ phase (0 and 10 vol% N2, Table 2) in Eq. (1) to obtain the dependence of $M_s$ on vol% $N_2$ in gas mixture during magnetron deposition:

$$M_s^{\alpha Fe}(\%N_2) = 1679 - 13.3 \cdot (\%N_2) \quad (2)$$

Using Eq. (2) the values of $M_s^{\alpha Fe}(\%N_2)$ were calculated for films with 13, 17 and 32% $N_2$ (Table 2), which were then substituted into the equation for the saturation magnetization of these films:

$$M_s = M_s^{Fe3O4} \cdot V_{Fe3O4} + M_s^{\alpha'} \cdot V_{\alpha'} + M_s^{\alpha Fe(N)} \cdot (100 - V_{Fe3O4} - V_{\alpha'}), \quad (3)$$

where $V_{\alpha'}$ is volume fraction of α′ phase, vol% (Fig. 2a). From Eq. (3) the saturation magnetization of the α′ phase $M_s^{\alpha'} = 1837 \pm 384$ G (2.31 ± 0.48 T, Table 2) was determined. Note that such a large error of $M_s^{\alpha'}$ is caused by two factors: the accuracy of determining the saturation magnetization of the films (Fig. 4a), which in turn strongly depends on

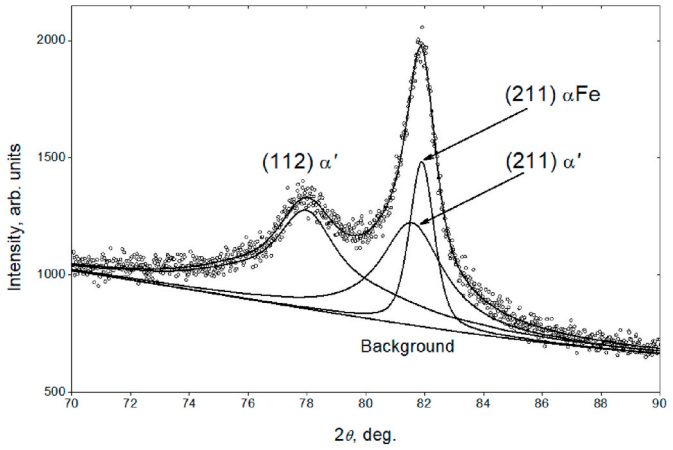


**Fig. 3.** Phase separation of αFe and α′ in the film with 32 vol% $N_2$ in gas mixture during magnetron deposition: dots are the experimental XRD data and the solid lines are fitting.

**Table 2**
The α′ lattice parameters ($a$ and $c$) and the saturation magnetization of α and α' phases.

| $N_2/(Ar + N_2)$, vol% | $a_{\alpha'}$, Å | $c_{\alpha'}$, Å | $M_s^{\alpha Fe}$, G | $M_s^{\alpha'}$, G (T) |
|---|---|---|---|---|
| 0 | – | – | 1679 ± 52 | – |
| 10 | – | – | 1546 ± 30 | – |
| 13 | 2.848 | 3.090 | 1520 ± 93 | 1981 ± 240 (2.49 ± 0.30) |
| 17 | 2.852 | 3.075 | 1444 ± 101 | 1771 ± 318 (2.23 ± 0.40) |
| 32 | 2.856 | 3.081 | 1253 ± 33 | 1747 ± 191 (2.20 ± 0.24) |

the accuracy of determining the thickness of the films (Table 1), and the dependence of $M_s^{\alpha'}$ on the nitrogen concentration in this phase (Table 2). It can be seen that with an increase in the $N_2$%, $M_s^{\alpha'}$ decreases, which is consistent with a change in the lattice parameter ($a$ and $c$, Table 2), i.e. with a decrease in the concentration of nitrogen in α' (see section 3.2). Thus, we cannot definitely compare $M_s^{\alpha'}$ with the values of pure αFe (2.15 T) [13] and ordered $Fe_{16}N_2$ (2.9 T) [17].

The coercive field $H_c$ monotonically rises with increasing nitrogen content from 68 ± 3 to 225 ± 10 Oe (Fig. 4b). Note that a decrease in the coercive field with increasing grain size of αFe (Fig. 4b) is uncharacteristic for nanocrystalline ferromagnets in which an inverse dependence $H_c \sim 2R_c^6$ is observed with a grain size of $2R_c$ less than the ferromagnetic exchange length [5]. The data of Fig. 4b we can only explain by the increase in the amount of α' phase (with a constant grain size, section 3.2) on $N_2$ increase in gas mixture during magnetron deposition, the magnetic anisotropy of which is unknown to us.

Further, we show that the coercive field $H_c$ (Figs. 4b and 5a), visible on the hysteresis loop, does not always correspond to the actual ferromagnetic phase. The shapes of hysteresis loops of the studied films indicate the presence of two modes of magnetic anisotropy in them. This fact is indicated by a "step" in a field about $H_c$ (Fig. 5a). To determine the coercive field of each of the magnetic anisotropies ($H_{c1}$ and $H_{c2}$), the loops were described by the empirical function (4) which can be considered as the modification of classical Langevin formula for magnetization process [18]. The experimentally determined magnetization (open symbols in Fig. 5a) is the algebraic sum of magnetization values corresponding to two hysteresis loops ($M_{s1}$ and $M_{s2}$) and the fictive paramagnetism ($\chi H$), which describes here the approximately linear beginning of approach to saturation:

$$M(H) = M_{s1}V_1(cth(P_1(H \pm H_{c1})) - (P_1(H \pm H_{c1})) - 1) + M_{s2}V_2(cth(P_2(H \pm H_{c2})) - (P_2(H \pm H_{c2})) - 1) + \chi H, \quad (4)$$

where $P_1$, $P_2$, $M_{s1}V_1$, $M_{s2}V_2$ and $\chi$ are the adjustable parameters. Note that the hysteresis loop is the magnetic moment of the sample divided by its volume. If there are two phases in a film with different saturation magnetizations, they are summed in proportion to their volume fractions $V_1$ and $V_2$. Since XRD gave us information about three ferromagnetic phases (the films with α′ phase, Fig. 2a), it is impossible to distinguish saturation magnetizations, i.e. $M_{s1}$ and $M_{s2}$ cannot be identified with specific quantities.

The magnetization curves of the studied films in the strong fields are fitted by the law of approaching to saturation magnetization [7,18].

$$M(H) = M_s\left[1 - (1/2)\left(D^{1/2}H_a\right)^2 \Big/ \left(H^2 + H^{1/2}H_R^{3/2}\right)\right], \quad (5)$$

from which the saturation magnetization $M_s$ (Fig. 4a), the rms fluctuation of the local (on the ferromagnetic grain scale) magnetic anisotropy field $D^{1/2}H_a$ ($D$ is dispersion of local anisotropy axes [7,19], which is unknown in this study) and exchange field $H_R$ ($H_R = 2A/M_sR_c^2$, where $A$ is exchange stiffness and $R_c$ is grain radius, Fig. 2b) are determined (Table 3).

$D^{1/2}H_a$ values for all studied films are equal to or lower than the exchange field $H_R$. According to Ref. [19], the exchange field is a threshold value of $D^{1/2}H_a$, below which ($D^{1/2}H_a < H_R$) the exchange interaction results in the formation of stochastic domains. Thus, the magnetic structure formed in the studied films consists of stochastic domains.

Using estimated $D^{1/2}H_a$ and $H_R$ values, the value of the 1st mode of anisotropy field of stochastic domains $D^{1/2}<H_a>_1$ [20,21] and their

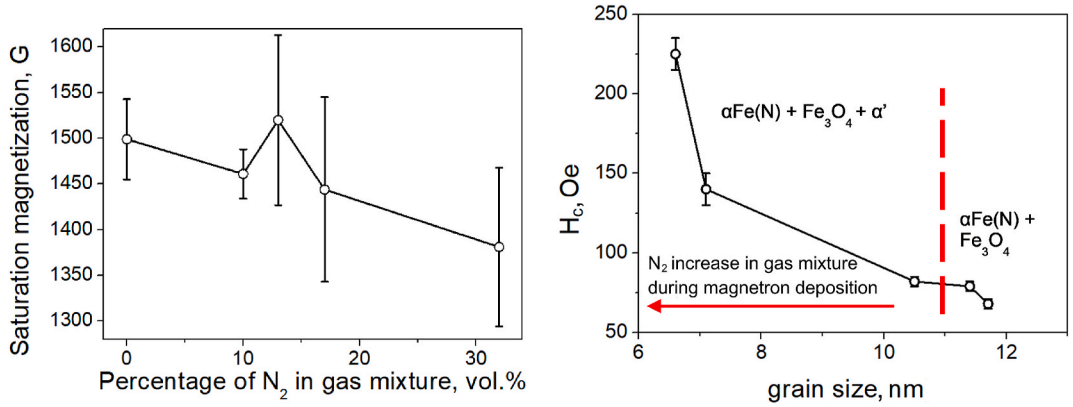


**Fig. 4.** The dependences of the saturation magnetization in the films under study on the concentration of $N_2$ in gas mixture during magnetron deposition (a) and the coercive field on the grain size of αFe(N) (b). Solid lines are guides for the eyes.

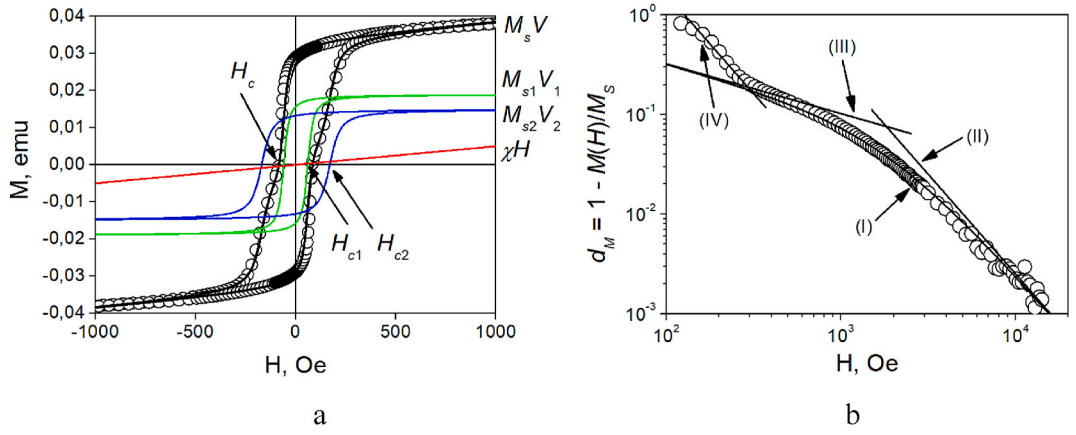


**Fig. 5.** The hysteresis loop (a) and the magnetization dispersion (b) of the film with 13% of $N_2$ in gas mixture during magnetron deposition.

**Table 3**
The parameters of stochastic domains in the films under study.

| $N_2/(Ar + N_2)$, vol% | $D^{1/2}H_a$, Oe | $H_R$, Oe | $R_{L1}/R_c$ | $R_{L2}/R_c$ |
|---|---|---|---|---|
| 0 | 714 ± 8 | 1816 ± 51 | 6.5 ± 0.5 | 4.5 ± 0.7 |
| 10 | 690 ± 6 | 1463 ± 40 | 4.5 ± 0.3 | 3.0 ± 0.3 |
| 13 | 708 ± 7 | 1817 ± 40 | 6.6 ± 0.4 | 3.2 ± 0.1 |
| 17 | 886 ± 34 | 784 ± 349 | 2.7 ± 0.9 | 0.8 ± 0.9 |
| 32 | 1139 ± 28 | 1492 ± 150 | 3.0 ± 0.4 | 1.7 ± 0.4 |

relative size $R_{L1}/R_c$ [21] were determined (Table 3) by

$$D^{1/2} < H_a >_1 = \left(D^{1/2}H_a\right)^4 \Big/ H_R{}^3 \text{ and} \tag{6}$$

$$R_{L1} / R_c = \left(H_R / D^{1/2}H_a\right)^2. \tag{7}$$

It should be noted that the obtained inequality $R_{L1}/R_c > 1$ for the studied films indicates the correctness of the consideration of their magnetic structure in terms of RAM [5,19].

The correlation magnetometry method [5,22] provides an opportunity to determine the $D^{1/2}H_a$ and $H_R$ parameters also by the graphical analysis of the magnetization dispersion $d_m = 1\text{-}M/M_s$ dependence on the external field $H$, which is plotted on log-log scale (Fig. 5b). Here, line *I*, described by Equation (5), has two asymptotes: *II* is described by $d_m=(1/2)\ (D^{1/2}H_a/H)^2$ (Akulov's law); *III* is described by $d_m=(1/2)\ (D^{1/2}H_a)^2/(H_R^{3/2}H^2)$ (the decrease in the stochastic domain size with increasing field), from which the $D^{1/2}H_a$ and $H_R$ values can be determined. $H_R$ is a field of intersection of the asymptotes *II* and *III*. Asymptote *IV* corresponding to a field range below few hundreds of oersteds is described by Ref. [22].

$$d_m = (1/2)\left(D^{1/2} < H_a >_2 / H\right)^2. \tag{8}$$

$H_L$ is a field of intersection of the asymptotes *III* and *IV*.

Using Eq. (8), the 2nd mode of anisotropy field of stochastic domains $D^{1/2}<H_a>_2$ was determined. As it is seen from Fig. 6, the $D^{1/2}<H_a>_2$ values exceed $D^{1/2}<H_a>_1$ by one order of magnitude. The fields $D^{1/2}<H_a>_1$ and $D^{1/2}<H_a>_2$ correlate well with coercive fields $H_{c1}$ and $H_{c2}$ (Fig. 6).

When assuming that the field $D^{1/2}<H_a>_2$ is determined for an area with the relative size [23]

$$R_{L2} \Big/ R_c = \left(H_R / D^{1/2} < H_a >_2\right)^{1/2}, \tag{9}$$

it follows that $R_{L1}/R_c > R_{L2}/R_c \geq 1$ (Table 3). The correlation magnetometry method assumes that average effective parameters $2R_c$, $M_s$, and $D^{1/2}H_a$ remain unchanged over the entire film volume, i.e. two modes of stochastic domains have the same $2R_c$, $M_s$, and $D^{1/2}H_a$, which follows

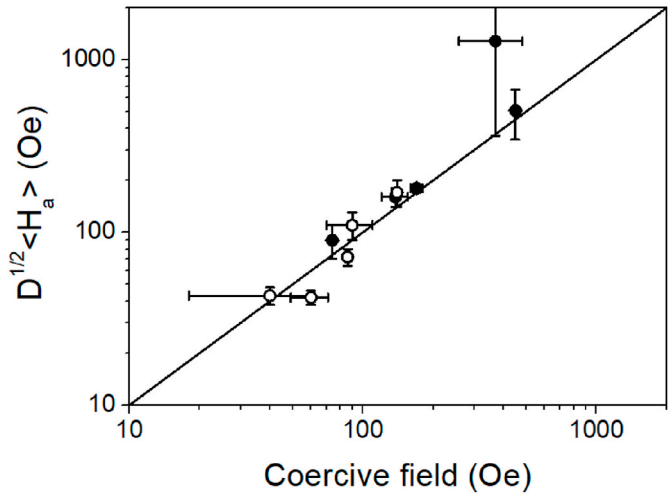


**Fig. 6.** The correlation of two coercive fields and two anisotropy fields of the stochastic domains in the films under study: ○ $H_{c1} \approx D^{1/2}<H_a>_1$; ● $H_{c2} \approx D^{1/2}<H_a>_2$. The solid line is $H_c = D^{1/2}<H_a>$.

from the fitting of magnetization curves by Eq. (5) and is approximately true for the structure from XRD (section 3.2).

Table 3 shows that in the films with the highest α′ phase content (17 and 32% $N_2$, Fig. 2a), one of the modes of stochastic domains has a size close to the grain size, $R_{L2}/R_c \approx 1$, therefore $H_{c2} \approx D^{1/2}<H_a>_2 \approx D^{1/2}H_a$. Thus the high coercive field (Fig. 4b) of these two films can be associated with the magnetic anisotropy of α' phase.

Thus, the α' phase can be characterized not only by the ordinary saturation magnetization relative to the α phase, but also by increased magnetic anisotropy.

## 4. Summary

The Fe–N–O films, which were deposited on glass substrates by reactive magnetron sputtering under different energy and gaseous atmosphere conditions, are studied.

All films contain impurity oxygen and nitrogen, which participate in the formation of the phase composition of the films.

The phase composition of the films under study, in accordance with the chemical composition, is various combinations of nanocrystalline phases (the grain sizes vary in a range of 5–12 nm in accordance with the chemical and phase composition of the films), such as αFe(N) solid solutions, α′ nitrous martensite, fcc $Fe_3O_4$ oxide. Some phenomena inherent for the non-equilibrium state of the films were found: the

formation of supersaturated interstitial αFe-based solid solution, precipitation of α' nitrous martensite with the bct crystal lattice.

The shapes of magnetic hysteresis loops indicate the presence of two main modes of coercive field in the studied Fe–N–O films. The magnetic structure of the films, is discussed in terms of RAM. The correlation magnetometry method was used to determine the parameters of the local (the magnetic anisotropy field within a grain $D^{1/2}H_a$) and macroscopic magnetic structure (the magnetic anisotropy field within a stochastic domain $D^{1/2}<H_a>$ and the stochastic domain radius $R_L$). It was found that two modes of the magnetic anisotropy field of stochastic domains $D^{1/2}<H_a>_1$ and $D^{1/2}<H_a>_2$ are formed, which determine the existence of two coercive fields.

The attempts have been made to determine the saturation magnetization of α' phase and the effect of its magnetic anisotropy on the coercive field and the magnetic structure of the Fe–N–O films.

## Declaration of competing interest

The authors declare that they have no known competing financial interests or personal relationships that could have appeared to influence the work reported in this paper.

## Acknowledgments

The reported magnetic measurements and analysis were funded by RFBR according to the research project N⁰18-32-00485mol_a ("Effective parameters of magnetic structure in nanocrystalline ferromagnetic bcc Fe-based films"). The reported XRD analysis was funded by the state order according to N⁰075 00746-19-00.

## References

[1] X. Peng, Sh Yu, J. Chang, M. Ge, J. Li, T. Ellis, Y. Yang, J. Xu, B. Hong, D. Jin, H. Jin, X. Wang, H. Ge, Preparation and magnetic properties of Fe4N/Fe soft magnetic composites fabricated by gas nitridation, J. Magn. Magn Mater. 500 (2020), 166407.

[2] M.H. Wetzel, M.R. Schwarz, A. Leineweber, High-pressure high-temperature study of the pressure induced decomposition of the iron nitride γ′-$Fe_4N$, J. Alloys Compd. 801 (2019) 438–448.

[3] Sh Atiq, H.-S. Ko, S.A. Siddiqi, S.-Ch Shin, Preparation and the influence of Co, Pt and Cr additions on the saturation magnetization of α″-$Fe_{16}N_2$ thin films, J. Alloys Compd. 479 (2009) 755–758.

[4] J. Liu, G. Guo, X. Zhang, F. Zhang, B. Ma, J.-P. Wang, Synthesis of α-$Fe_{16}N_2$ foils with an ultralow temperature coefficient of coercivity for rare-earth-free magnets, Acta Mater. 184 (2020) 143–150.

[5] G. Herzer, Modern soft magnets: amorphous and nanocrystalline materials, Acta Mater. 61 (2013) 718–734.

[6] E.V. Shelekhov, T.A. Sviridova, Programs for X-ray analysis of polycrystals, Met. Sci. Heat Treat. 42 (2000) 309–313.

[7] S.V. Komogortsev, R.S. Iskhakov, Law of approach to magnetic saturation in nanocrystalline and amorphous ferromagnets with improved transition behavior between power-law regimes, J. Magn. Magn Mater. 440 (2017) 213–216.

[8] V.A. Shabashov, S.V. Borisov, A.E. Zamatovsky, N.F. Vildanova, A.G. Mukoseev, A. V. Litvinov, O.P. Shepatkovsky, Deformation-induced transformations in nitride layers formed in bcc iron, Mater. Sci. Eng. 452–453 (2007) 575–583.

[9] H.A. Wriedt, N.A. Gokcen, R.H. Nafziger, The Fe-N (Iron-Nitrogen) system, Bulletin of Alloy Phase Diagrams 8 (1987) 355–377.

[10] A.N. Timoshevskii, B.Z. Yanchitsky, Ordering effects and hyperfine interactions in Fe-N Austenites, Hyperfine Interact. 158 (2004) 111–115.

[11] M.F.R. Fouda, R.S. Amin, M. Hassanein, Thermal and spectroscopic characterization of Mn(II), Fe(II) and Fe(III) diphenylcarbazonate complexes, Thermochim. Acta 145 (1989) 281–289.

[12] D. Nicholls, The Chemistry of Iron, Cobalt and Nickel, first ed., Pergamon Press, Oxford, 1973, p. 1010.

[13] E.N. Sheftel, E.V. Harin, Fe-Zr-N films: effect of nitrogen content and nitrogen-to-zirconium concentration ratio on saturation induction, Mater. Lett. 229 (2018) 36–39.

[14] D.S. Rickerby, A.M. Jones, B.A. Bellamy, X-ray diffraction studies of physically vapour-deposited coatings, Surf. Coating. Technol. 37 (1989) 111–137.

[15] F. Vaz, L. Reboutaa, Ph Goudeau, T. Girardeau, J. Pacaud, J.P. Riviére, A. Traverse, Structural transitions in hard Si-based TiN coatings: the effect of bias voltage and temperature, Surf. Coating. Technol. 146–147 (2001) 274–279.

[16] M. Sun, A. Zhun, Q. Zhang, Q. Liu, A facile strategy to synthesize monodisperse superparamagnetic OA-modified $Fe_3O_4$ nanoparticles with PEG assistant, J. Magn. Magn Mater. 369 (2014) 49–54.

[17] M. Takahashi, H. Shoji, α″-$Fe_{16}N_2$ problem — giant magnetic moment or not, J. Magn. Magn Mater. 208 (2000) 145–157.

[18] S.V. Komogortsev, E.A. Denisova, R.S. Iskhakov, A.D. Balaev, L.A. Chekanova, YuE. Kalinin, A.V. Sitnikov, Multilayer nanogranular films $(Co_{40}Fe_{40}B_{20})_{50}(SiO_2)_{50}$/α-Si:H and $(Co_{40}Fe_{40}B_{20})_{50}(SiO_2)_{50}/SiO_2$: magnetic properties, J. Appl. Phys. 113 (2013), 17C105.

[19] R.S. Iskhakov, S.V. Komogortsev, Magnetic microstructure of amorphous, nanocrystalline, and nanophase ferromagnets, Phys. Met. Metallogr. 112 (2011) 666–681.

[20] E.M. Chudnovsky, Magnetic properties of amorphous ferromagnets (invited), J. Appl. Phys. 64 (1988) 5770.

[21] R.S. Iskhakov, S.V. Komogortsev, Zh M. Moroz, E.E. Shalygina, Characteristics of the magnetic microstructure of amorphous and nanocrystalline ferromagnets with a random anisotropy: theoretical estimates and experiment, JETP Lett. (Engl. Transl.) 72 (2000) 603–607.

[22] R.S. Iskhakov, S.V. Komogortsev, Magnetic microstructure of nanostructured ferromagnets, Bull. Russ. Acad. Sci. Phys. 71 (2007) 1620–1622.

[23] R.S. Iskhakov, V.A. Ignatchenko, S.V. Komogortsev, A.D. Balaev, Study of magnetic correlations in nanostructured ferromagnets by correlation magnetometry, JETP Lett. (Engl. Transl.) 78 (2003) 646–650.